



Figures and figure supplements

Selective endocytosis controls slit diaphragm maintenance and dynamics in *Drosophila* nephrocytes

Konrad Lang et al

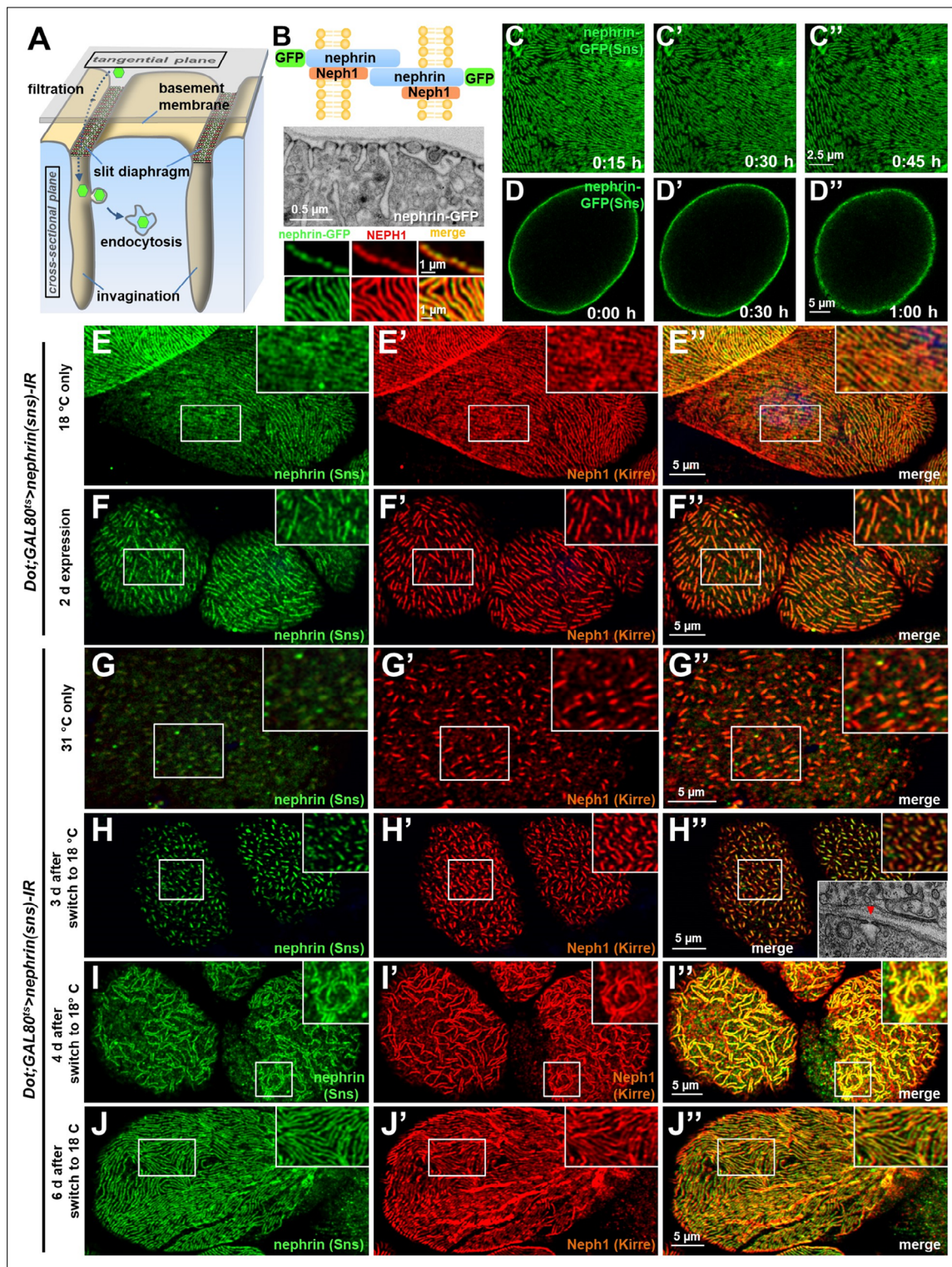


Figure 1. Slit diaphragm proteins form a stable architecture that is re-established upon disruption. **(A)** Schematic illustrating the nephrocyte ultrastructure and function (surface detail). Molecules destined for removal (shown as green hexagons) pass a bi-layered filtration barrier before being subject to endocytosis within membrane invaginations. **(B)** The schematic (upper section) illustrates the slit diaphragm after knock-in of GFP into the nephrin locus. The transmission electron microscopy image (middle section) shows a surface detail of a nephrocyte expressing nephrin-GFP homozygously with regular slit diaphragms. Confocal images (lower section) of a nephrin-GFP nephrocyte show colocalization with endogenous Neph1 (Kirre) in cross-sectional (upper row) and tangential sections (lower row). **(C–D'')** Snapshots from a movie obtained by live-cell imaging reveal a stable slit diaphragm pattern in the tangential section **(C–C'')**. This is confirmed by cross-sectional analysis in the same genotype **(D–D'')** where no vesicles for

Figure 1 continued on next page

Figure 1 continued

bulk transport of nephrin are observed. **(E–F’)** Confocal images of tangential section of nephrocytes stained for slit diaphragm proteins while silencing of fly nephrin (*sns*) is blocked by *GAL80^{ts}* at 18°C show a regular staining pattern **(E–E’)**. A temperature shift to 31°C initiates RNAi expression, resulting in reduction of approximately 50% of the slit diaphragm protein after 2 days **(F–F’)**. **(G–I’)** Confocal images of tangential section of nephrocytes that express nephrin (*sns*)-RNAi and *GAL80^{ts}* continuously at a non-inhibiting temperature of 31°C stained for slit diaphragm proteins nephrin (*sns*) and Neph1 (Kirre) show an extensive loss of nephrin staining after silencing while a punctate pattern of Neph1 (lacking its binding partner) is observed (see also magnified inset) **(G–G’)**. Both proteins colocalize in short lines indicating renewed formation of slit diaphragms after a temperature shift to 18°C that inhibits RNAi expression for 3 days **(H–H’)**. Inset in **(H’)** shows transmission electron microscopy of the same stage with return of sparse and isolated slit diaphragms (red arrowhead). The longer lines of slit diaphragm proteins begin to cluster in pairs or triplets after another day, covering a large part of the cell surface in a wide-meshed network **(I–I’)**. **(J–J’)** Slit diaphragm architecture is restored after blocking the expression of nephrin-RNAi for 6 days.

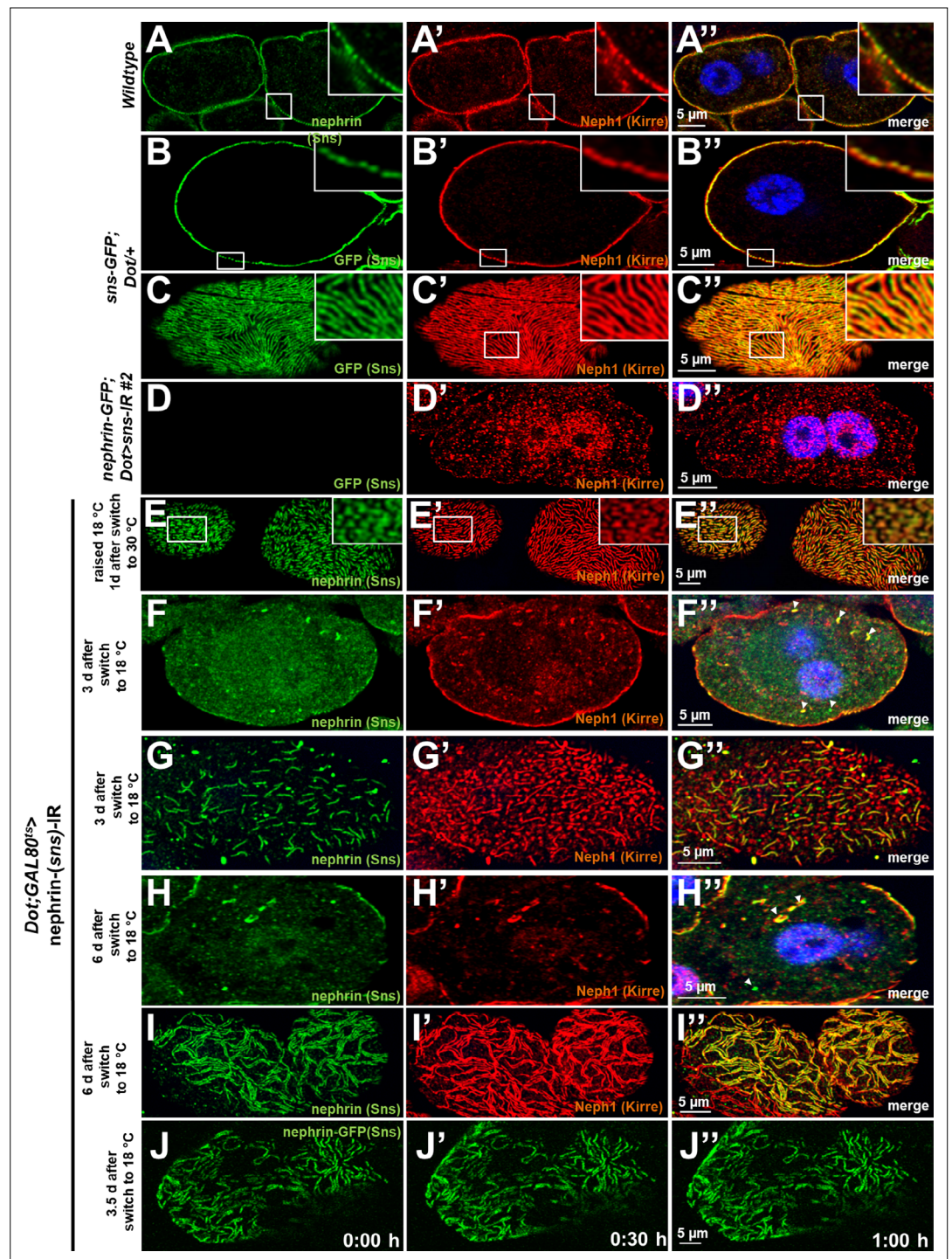


Figure 1—figure supplement 1. Validation of nephrin-GFP and additional time points for disruption and reassembly of slit diaphragms. (A) Cross section of a control garland cell nephrocyte (+/+) co-stained for nephrin (Sns) and Neph1 (Kirre). Nuclei are marked by Hoechst 33342 in blue here and throughout the figure. (B–D'') GFP-derived signal of nephrocytes from animals carrying genomic nephrin-GFP homozygously matches the regular slit diaphragm pattern of endogenous Neph1 in cross sections (B–B'') and tangential sections (C–C'') but is abrogated upon silencing of fly nephrin (D–D''). (E–E'') Lines of slit diaphragm proteins begin to shorten after 24 hr of fly nephrin silencing. (F–I'') Fly nephrin is still strongly reduced 3 days after expression of RNAi against fly nephrin has been inhibited by a temperature shift to 18°C (F–F''). Neph1 (Sns) begins to return with lines elongating while fly Neph1 resides mostly in punctae after 4 days (G–G''). Slit diaphragms cover most of the cell surface in clustered lines 6 days after the temperature shift (H–I''). Arrowheads indicate intracellular nephrin/Neph1. (J–J'') Live-cell Figure 1—figure supplement 1 continued on next page

Figure 1—figure supplement 1 continued

imaging of nephrin-GFP nephrocytes 3.5 days after transient silencing of nephrin shows reconstitution occurs at a slow rate.

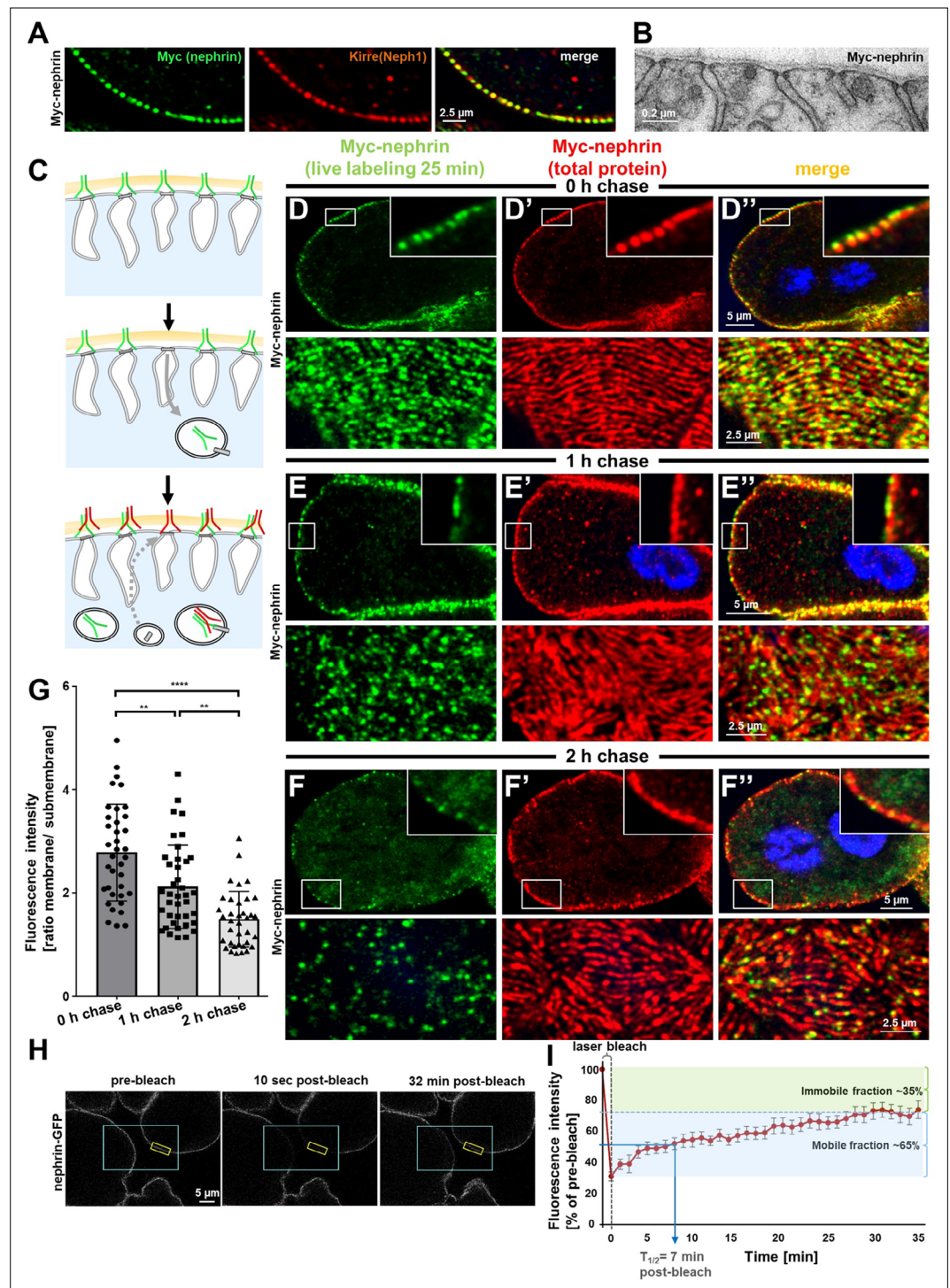


Figure 2. Live antibody labeling shows rapid nephrin turnover. **(A)** Immunostaining of nephrocyte expressing Myc-nephrin homozygously shows colocalization with endogenous Neph1. **(B)** Transmission electron microscopy of a nephrocyte expressing Myc-nephrin homozygously reveals regular slit diaphragms suggesting the tagged protein is functional. **(C)** Schematic illustrating live antibody labeling: Living nephrocytes are labeled with anti-Myc antibody (green) that may undergo endocytosis during chasing. Total nephrin stain follows after fixation and permeabilization (red). Colocalization of green and red indicates stable nephrin (surface) or endocytosed nephrin (subcortical). Exclusively green signal indicates antibody dissociation, while new nephrin reaching the surface during the chase period will stain only red. **(D)** Confocal microscopy images show cross sections (top) and tangential sections (bottom) from Myc-nephrin nephrocytes after live antibody labeling without chasing.

Figure 2 continued on next page

Figure 2 continued

Extensive colocalization indicates successful nephrin labeling. Nuclei are marked by Hoechst 33342 in blue here and throughout the figure. **(E)** Confocal images analogous to **(D)** but after 1 hr of chasing reveal incipient endocytosis. **(F)** Confocal images analogous to **(D–D'')** but after 2 hr of chasing suggest extensive endocytosis. Diffuse intracellular signal from live labeling suggests that internalized antibody separated from nephrin. Exclusively red nephrin signal indicates newly delivered protein. **(G)** Quantitation of fluorescence intensity derived from live labeling from conditions in **(D–F)** expressed as a ratio of surface (slit diaphragm) and subcortical areas confirms significant nephrin turnover (mean \pm standard deviation, $n=12–13$ animals per $p<0.01$ for chase of 1 hr and $p<0.0001$ for 2 hr). **(H)** Shown are frames from a time lapse movie of nephrin-GFP nephrocytes. The blue box demarcates the region of photobleaching, the yellow box outlines a region of interest (ROI) where the fluorescence intensity was measured over the length of the fluorescence recovery after photobleaching (FRAP) experiment. A loss of fluorescence intensity compared to pre-bleach condition (left panel) is detectable 10 s after photobleaching (middle panel). After 32 min, the fluorescence recovers significantly (right panel). **(I)** Quantitative analysis from multiple FRAP experiments ($n=5$ cells, 8 ROIs total, mean \pm standard deviation) reveals an initially rapid recovery of fluorescence intensity that slows to a plateau suggesting a nephrin half-life of ~ 7 min. The majority of nephrin molecules ($\sim 65\%$) are replaced within 30 min (mobile fraction).

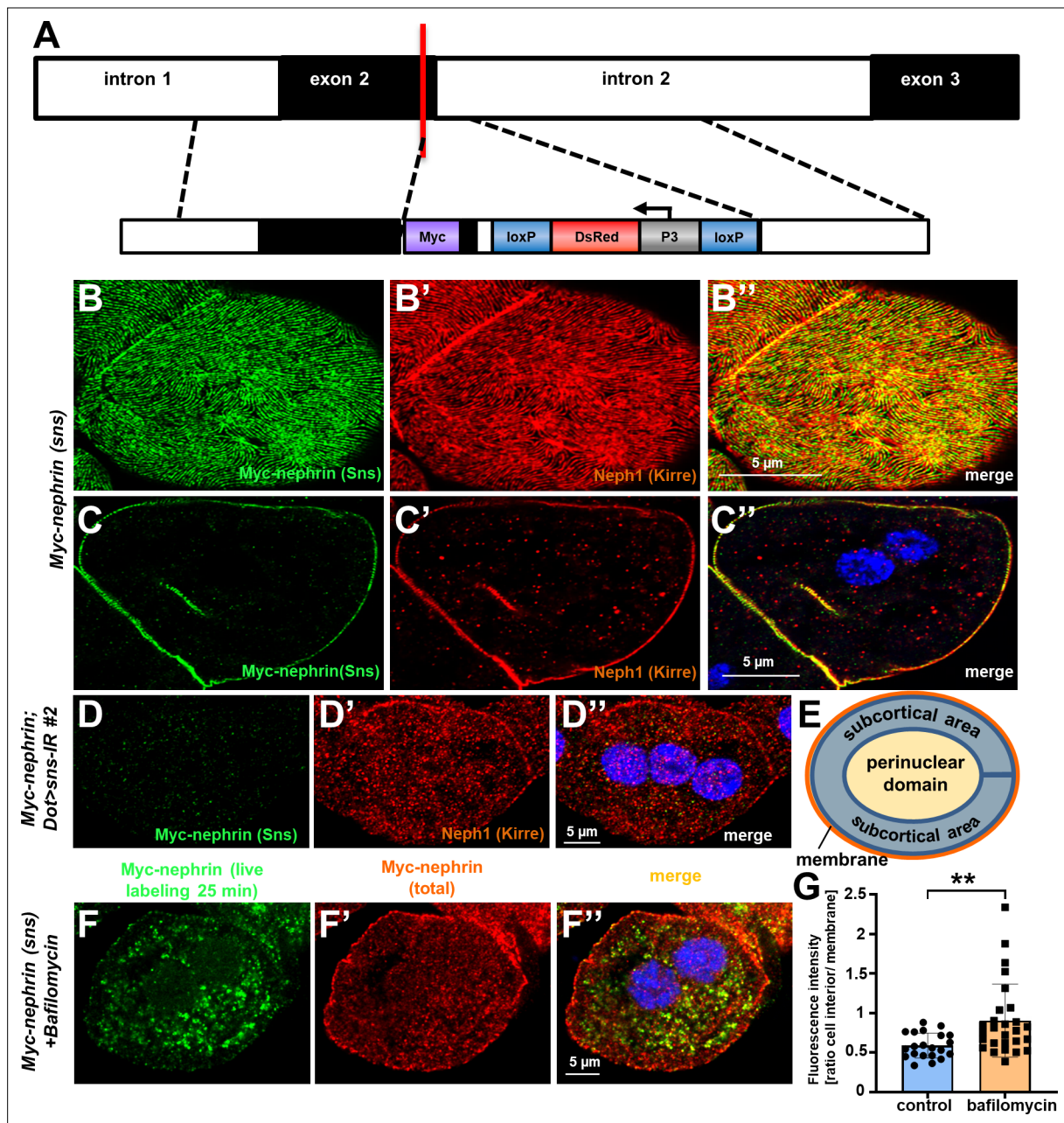


Figure 2—figure supplement 1. Validation of Myc-nephrin and bafilomycin treatment. **(A)** Shown is a schematic that indicates the genome editing strategy of introducing a myc-tag into the extracellular domain of *sns*, the fly nephrin. While myc is targeted to the border of exon 2, a marker (in reverse orientation) is inserted into the flanking intron. The marker expresses Dsred under control of the P3 promoter for identification of genome-edited flies, but is removable by flanking loxP sites. **(B–C'')** Shown are a tangential section (**B–B''**) and a cross section (**C–C''**) of a garland cell nephrocyte that carries Myc-tag in frame within the locus of fly nephrin, stained for Myc and Neph1 (Kirre). The Myc staining reveals a highly specific staining in a typical fingerprint-like pattern and colocalizes with endogenous fly Neph1. Nuclei are marked by Hoechst 33342 in blue here and throughout the figure. **(D–D'')** Silencing fly nephrin abrogates the specific signal from Myc-staining, confirming that the Myc staining indeed reflects endogenously expressed Myc-nephrin. **(E)** Schematic drawing of the areas used for the quantitation in **Figures 2G and 5L** (membrane = orange and subcortical area = blue). **(F–F'')** A nephrocyte after live antibody labeling and chase of 120 min in presence of bafilomycin (0.1 μ M) is shown. This treatment causes a scattered, vesicular signal in the cytosol (**F**) that partially colocalizes with total nephrin (**F–F''**), suggesting retention of the endocytosed antibody after blocking lysosomal degradation. **(G)** Quantification of the results from (**F–F''**) compared to a control treatment without bafilomycin and shown as an intensity ratio of the cell interior vs. membrane ($n=8-10$ per genotype, $p<0.01$ for bafilomycin 0.1 μ M).

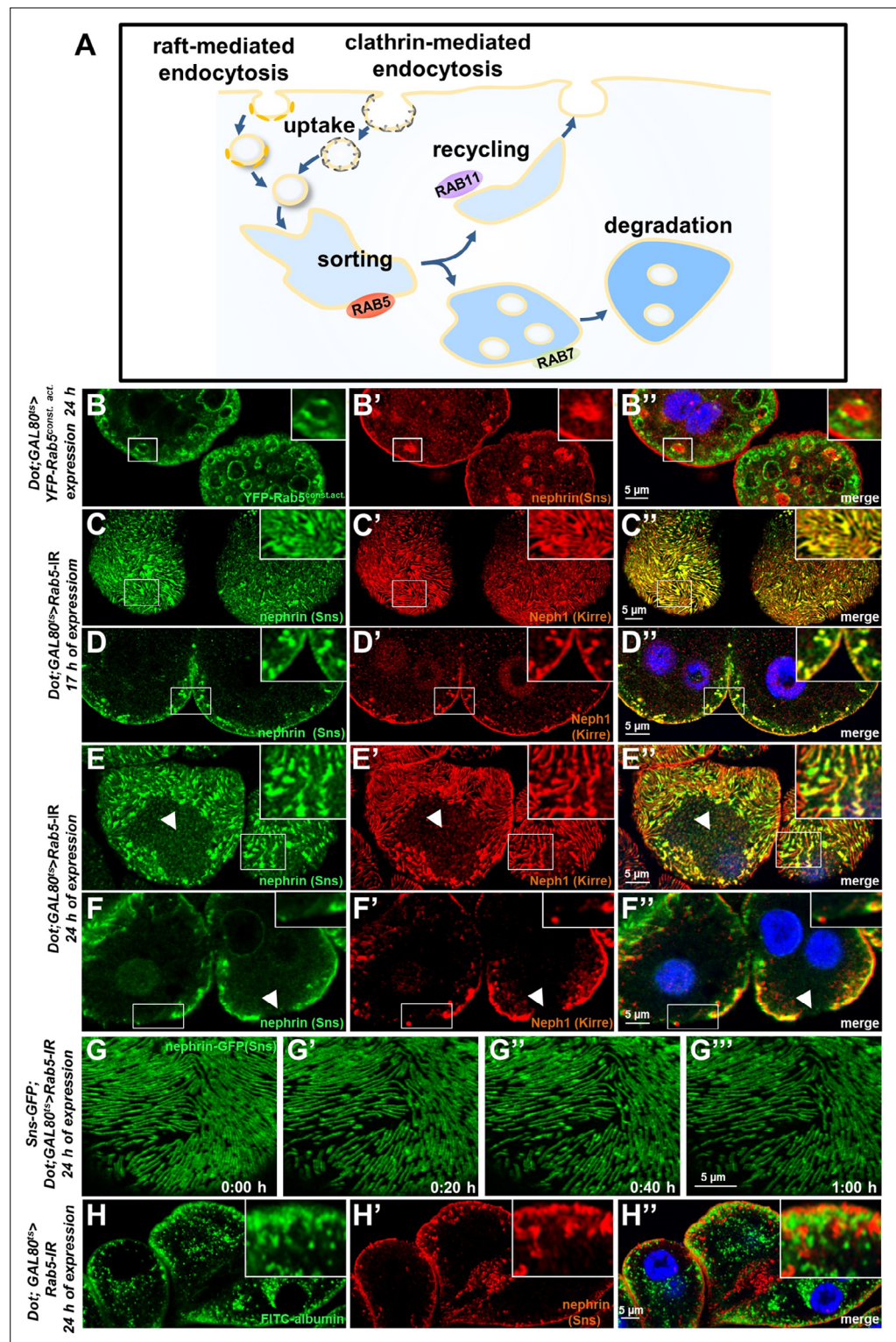


Figure 3. Endosomal regulator Rab5 is required for maintenance of slit diaphragms. **(A)** Schematic illustrating endocytic trafficking in a simplified manner shows raft-mediated and clathrin-mediated uptake converging in the early endosome by vesicle fusion. Uptake, early endosome formation and cargo sorting are controlled by Rab5. Sorting may direct cargo either toward degradation, which is promoted by Rab7, or back toward the cell membrane by recycling pathways such as Rab11-dependent recycling. **(B–B’)** Cross-sectional confocal microscopy images from nephrocytes expressing constitutively active YFP-Rab5 for 24 hr (green) show highly enlarged early endosomes that contain ectopic fly nephrin (see also magnified inset). Nuclei are marked by Hoechst 33342 in

Figure 3 continued on next page

Figure 3 continued

blue here and throughout the figure. **(C)** Confocal images of nephrocytes with acute silencing of *Rab5* for 17 hr reveals brighter sections within the lines of slit diaphragm protein in tangential sections. Lines further are blurry and focally confluent (see also magnified inset). **(D)** Cross-sectional images of nephrocytes with short-term silencing of *Rab5* show appearance of ectopic slit diaphragm protein below the surface (compare to control **Figure 3—figure supplement 1A-A'**). **(E–F)** Tangential sections **(E)** and cross sections **(F)** of nephrocytes with slightly longer silencing of *Rab5* for 24 hr stained for nephrin (Sns) and Neph1 (Kirre) reveal progressive thickening of slit diaphragms and localized breakdown of the slit diaphragms in a circumscribed area (white arrowheads). **(G–G''')** Snapshots from a movie obtained by live-cell imaging using confocal microscopy are shown. Nephrocytes expressing nephrin-GFP (heterozygously) are shown after 24 hr of acute *Rab5* silencing. Increasing gaps and a progressive reduction of slit diaphragms are observed over the course of 1 hr. Cells with a mild phenotype were chosen for live-cell imaging to ensure cellular viability. The nephrin signal in tangential sections appears slightly less blurry compared to untagged nephrin. **(H–H''')** Confocal microscopy images showing cross sections of nephrocytes after 24 hr of *Rab5* silencing are shown. Living cells were exposed to FITC-albumin (green) for 15 min before fixation and staining for nephrin (red). Cells show significant endocytosis of FITC-albumin indicating cell viability and residual endocytic activity despite silencing of *Rab5*. Ectopic nephrin and FITC-albumin do not colocalize, indicating that ectopic nephrin is not found within a subcellular compartment that is also destination for recently endocytosed cargo.

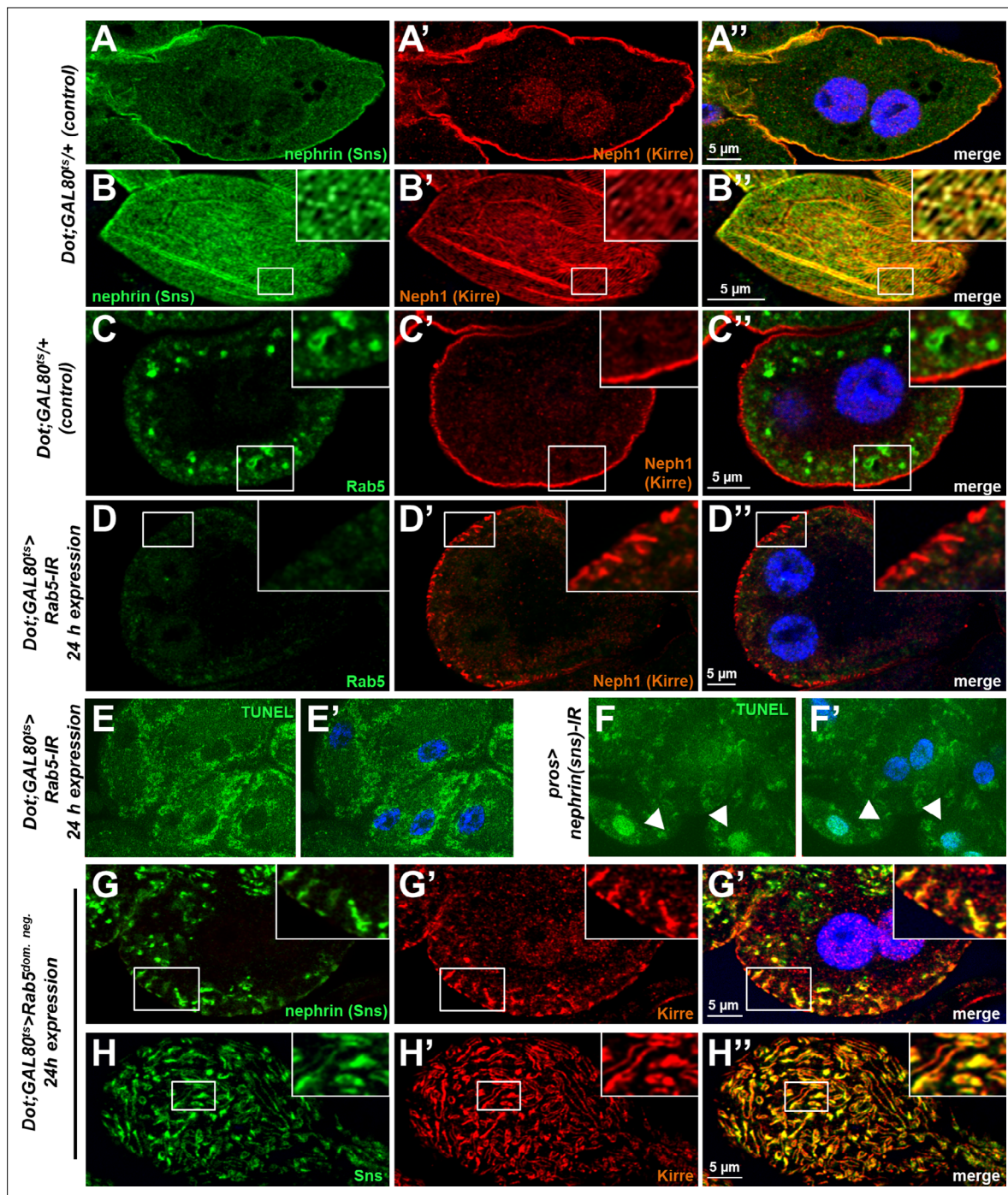


Figure 3—figure supplement 1. Validation and control experiments for loss-of-function of Rab5. (A–B'') Shown are a cross section (A–A'') and a tangential section (B–B'') of a garland cell nephrocyte that expresses *GAL80^{ts}* alone, stained for Nephrin (Sns) and Neph1 (Kirre). Nuclei are marked by Hoechst 33342 in blue here and throughout the figure. (C–D'') Rab5 stains in small vesicles at the cell periphery in control nephrocytes (C–C''). Silencing *Rab5* strongly diminishes the Rab5 signal and fly Neph1 reveals mislocalization. This indicates that short-term silencing is sufficient for a significant knockdown of Rab5. (E–F') Nephrocytes expressing *Rab5*-RNAi for 24 hr were subject to transferase dUTP nick end labeling (TUNEL) staining but no specific signal from the nuclei is observed (E, compare to Hoechst 33342 in E'), indicating that cells are not apoptotic. In contrast, when silencing fly nephrin as a positive control, we observed appearance of TUNEL-positive cells (F–F'). (G–H'') Nephrocytes with short-term expression of a dominant negative *Rab5* for 24 hr show ectopic slit diaphragm protein below the surface in cross sections (G–G'') and blurry and confluent lines of slit diaphragm protein in tangential sections (H–H'').

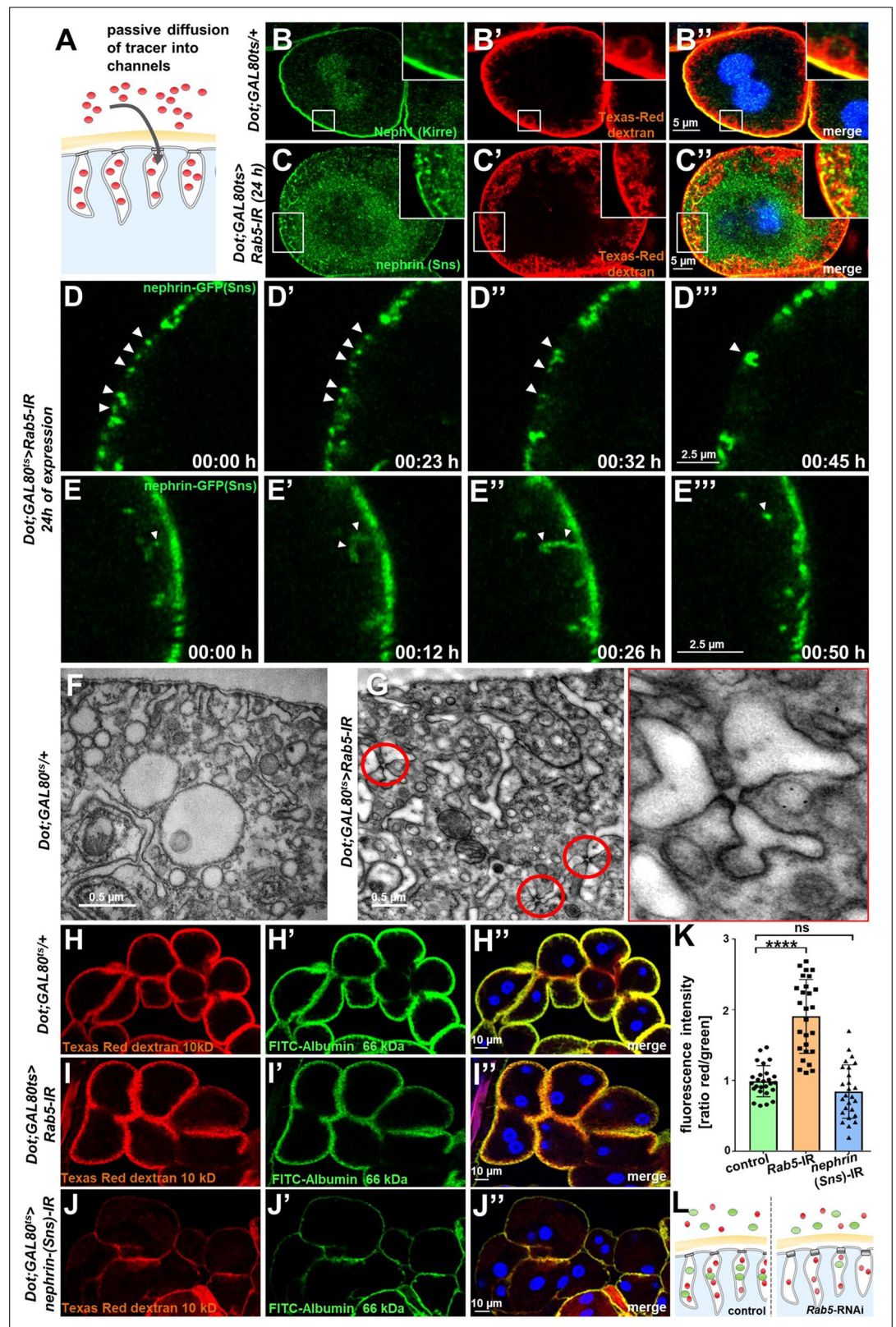


Figure 4. Endocytosis prevents lateral diffusion of nephrin and preserves filter permeability. **(A)** Schematic illustrates the assay for visualization of labyrinthine channels. Nephrocytes are fixed briefly before exposure to Texas-Red-Dextran that enters the channels by passive diffusion. **(B)** Confocal microscopy image of a control nephrocyte is stained for Neph1 (green) together with labeling of the channels by Texas-Red-Dextran (10 kDa, Figure 4 continued on next page

Figure 4 continued

red). Channels extend directly below the slit diaphragms. Nuclei are marked by Hoechst 33342 in blue here and throughout the figure. **(C)** Confocal images of nephrocytes with short-term silencing of *Rab5* show mislocalized fly nephrin below the cell surface that colocalizes significantly with the labyrinthine channels visualized by Texas-Red-Dextran (10 kDa). **(D–E''')** Snapshots from movies obtained by live-cell imaging are shown. Nephrocytes express nephrin-GFP (heterozygously) concomitant with *Rab5*-RNAi for 24 hr. Fusion and cluster formation (white arrowheads in panels D) of fly nephrin precedes appearance of gaps **(D–D''')**. Similarly, formation of protrusions of slit diaphragm proteins from the cell surface is followed by a formation of vesicles **(E–E''')**, white arrowheads). **(F)** Electron microscopy (EM) image from a cross section through the surface of a control nephrocyte reveals regular slit diaphragms bridging the membrane invaginations called labyrinthine channels. **(G)** EM image from a section through the surface of a nephrocyte expressing *Rab5*-RNAi acutely for 24 hr demonstrates ectopic formation of slit diaphragms forming rosette-like structures within the labyrinthine channels (red circles, magnification on the right). **(H–J''')** Confocal microscopy images of nephrocytes after simultaneous uptake of tracers FITC-albumin (66 kDa, green) and Texas-Red-Dextran (10 kDa) are shown. Control nephrocytes show robust uptake of both tracers **(H–H''')**. Silencing of *Rab5* acutely for 24 hr shows a stronger decrease in the uptake of the larger tracer FITC-albumin compared to smaller Texas-Red-Dextran **(I–I''')**. Both tracers are equally reduced upon *nephrin* silencing **(J–J''')**. **(K)** Quantitation of fluorescence intensity expressed as a ratio of Texas-Red-Dextran/FITC-albumin (small/large tracer) confirms a disproportionate reduction for the larger tracer for *Rab5*-RNAi but not *nephrin*-RNAi (mean \pm standard deviation, $n=9$ animals per genotype, $p<0.0001$ for *Rab5*-RNAi, $p>0.05$ for *nephrin*-RNAi). **(L)** Schematic illustrates how incipient filter clogging affects uptake of larger tracer disproportionately.

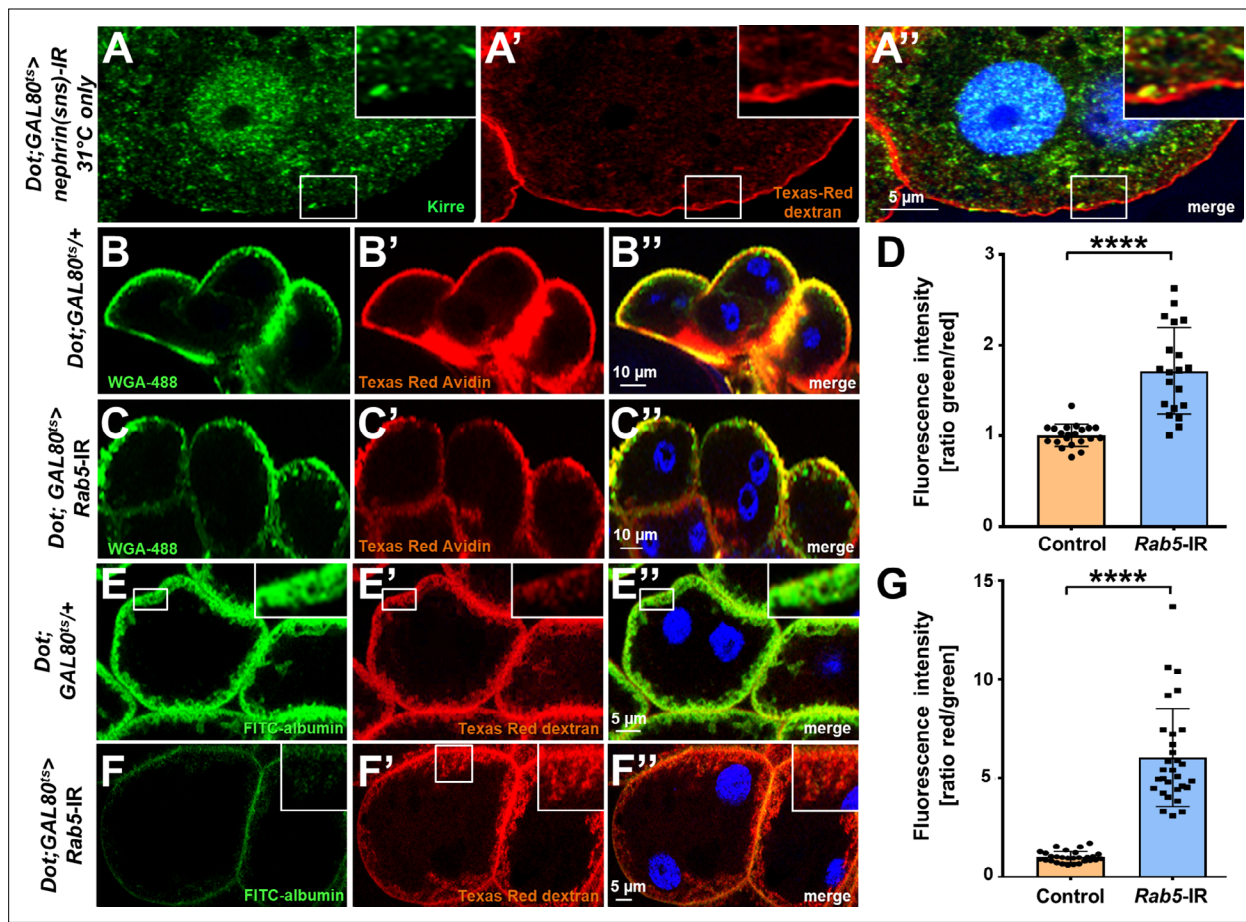


Figure 4—figure supplement 1. Channel diffusion assay reveals loss of invaginations upon silencing of nephrin and impaired slit diaphragm passage upon silencing of *Rab5*. (A–A'') Shown is a cross section (A–A'') of a garland cell nephrocyte subject to the channel diffusion assay. Texas-Red-Dextran does not penetrate deeper into the cell when channels are abrogated by expression nephrin (*Sns*)-RNAi, supporting that the signal is specific for the membrane invaginations called labyrinthine channels. Nuclei are marked by Hoechst 33342 in blue here and throughout the figure. (B–C'') Confocal microscopy image of nephrocytes after simultaneous uptake of Alexa Fluor 488 wheat germ agglutinin (38 kDa, green) and the larger tracer Texas-Red-Avidin (66 kDa) for control nephrocytes (B) and after silencing *Rab5* (C), which has a weaker impact on uptake of the smaller tracer. (D) Quantitation of fluorescence intensity expressed as a ratio of WGA-488/Texas-Red-Avidin (small/large tracer) confirms disproportionate reduction for the larger tracer upon expression of *Rab5*-RNAi (mean \pm standard deviation $n=7$ animals per genotype, $p<0.0001$ for *Rab5*-RNAi). (E–F'') The channel assay reveals a greater reduction in FITC-albumin penetration into channels compared to the smaller Texas-Red-Dextran (10 kDa) for silencing of *Rab5* (F–F'') compared to the control (E–E''). (G) Quantitation of fluorescence intensity expressed as a ratio of Texas-Red-Dextran/FITC-albumin (small/large tracer) further confirms the described disbalanced reduction for the larger tracer for *Rab5*-RNAi (mean \pm standard deviation, $n=9$ animals per genotype, $p<0.0001$ for *Rab5*-RNAi).

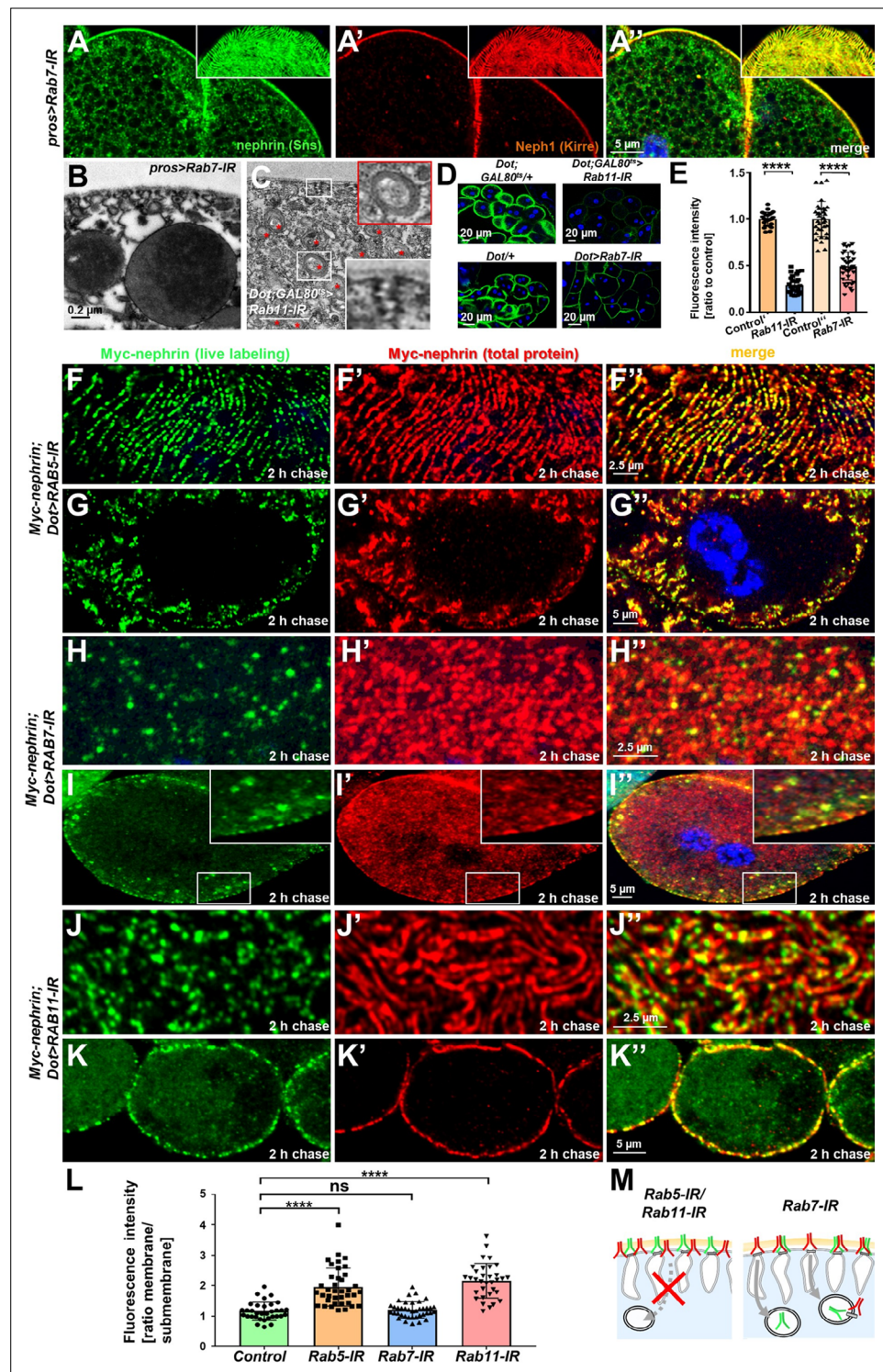


Figure 5 continued

shows reduced uptake for *Rab7*-RNAi (lower panels) and *Rab11*-RNAi (upper panels) using *Dorothy*-GAL4 or *prospero*-GAL4 compared to the respective controls. **(E)** Quantitation of results from **(D)** in ratio to a control experiment performed in parallel (mean \pm standard deviation, $n=11-14$ animals per genotype, $p<0.0001$ for *Rab7*-RNAi and $n=9$ animals per genotype $p<0.0001$ for *Rab11*-RNAi). Sidak post hoc analysis was used to correct for multiple comparisons. **(F-K'')** Confocal microscopy images of tangential sections **(F-F'', H-H'', J-J'')** and cross sections **(G-G'', I-I'', K-K'')** of Myc-nephrin nephrocytes after live antibody labeling and 2 hr of chasing are shown for the indicated genotypes. Silencing of *Rab5* at 18°C was obtained before flies were adapted to 25°C for 1 hr **(F-G'')**. Live labeling (green) and total stain (red) show near-complete colocalization for *Rab5*-RNAi **(F-G'')**, indicating disrupted nephrin turnover. Extensive amounts of subcortical nephrin are revealed in cross sections **(G-G'')**, compatible with lateral diffusion into the membrane invaginations. Cells expressing *Rab7*-RNAi after live antibody labeling show undisturbed nephrin turnover as the live labeled antibody is removed from the surface **(H-H'')**. Cross sections of *Rab7*-RNAi nephrocytes reveal numerous subcortical vesicles that partially show isolated signal for the live labeling, indicating the antibody disengaged from nephrin **(I-I'')**. Nephrocytes expressing *Rab11*-RNAi show strong retention of live labeled nephrin on the cell surface **(J-J'')**, suggesting impaired turnover. Cross sections show the antibody on the surface, but not in labyrinthine channels **(K-K'')**. **(L)** Quantitation of results from **(F-K'')** expressed as ratio of the fluorescence intensity between surface and subcortical region for individual cells (mean \pm standard deviation, $n=11-13$ animals per genotype, $p<0.0001$ for *Rab5*-RNAi, $p>0.05$ for *Rab7*-RNAi and $p<0.0001$ for *Rab11*-RNAi). **(M)** Schematic illustrates findings studying nephrin live labeling upon silencing of *Rab5/Rab7/Rab11*.

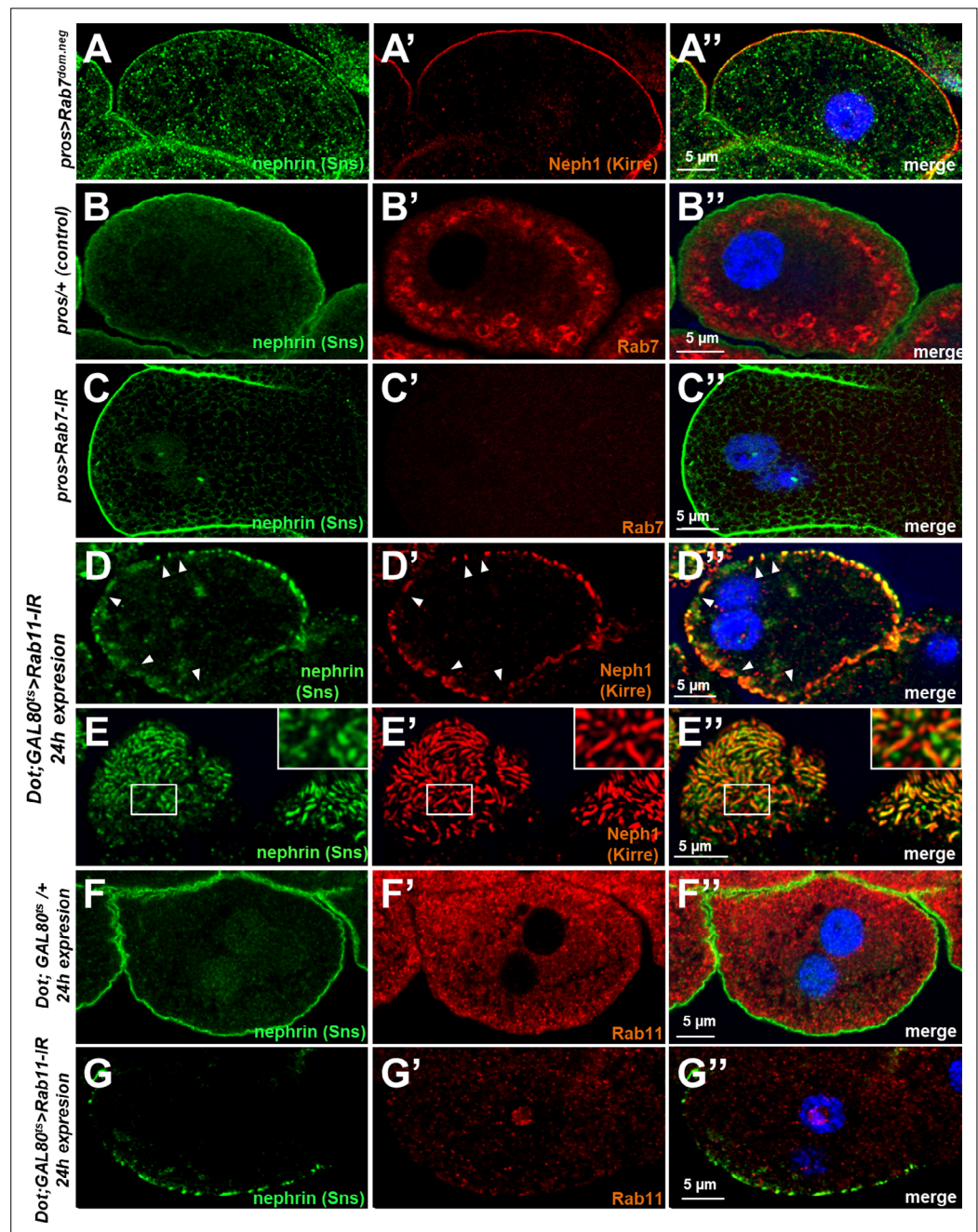


Figure 5—figure supplement 1. Validation and controls for *Rab7* and *Rab11*. (A–A'') Slit diaphragms are formed regularly upon expression of dominant negative *Rab7*, while nephrin accumulates diffusely in the cell. Fly *Neph1* is less affected than fly nephrin upon silencing of *Rab7*. (B–B'') Control nephrocytes expressing *prospero-GAL4* alone (B–B'') show the regular staining pattern of fly nephrin (Sns) and *Rab7*. Signal of the *Rab7* antibody is lost upon expression of *Rab7-RNAi* (C–C''). (D–E'') Acute silencing of *Rab11* for 24 hr in nephrocytes results in coarser, wider spaced dots in cross sections (D–D'') matching wider gaps between the lines of slit diaphragm proteins in tangential sections (E–E''). Slit diaphragm proteins may occasionally occur independently from each other (inset in E–E''). (F–G'') Short-term expression of *Rab11-RNAi* strongly diminishes the signal derived from an antibody raised against human *Rab11* (compare F–F'' to G–G'') suggesting an efficient knockdown.

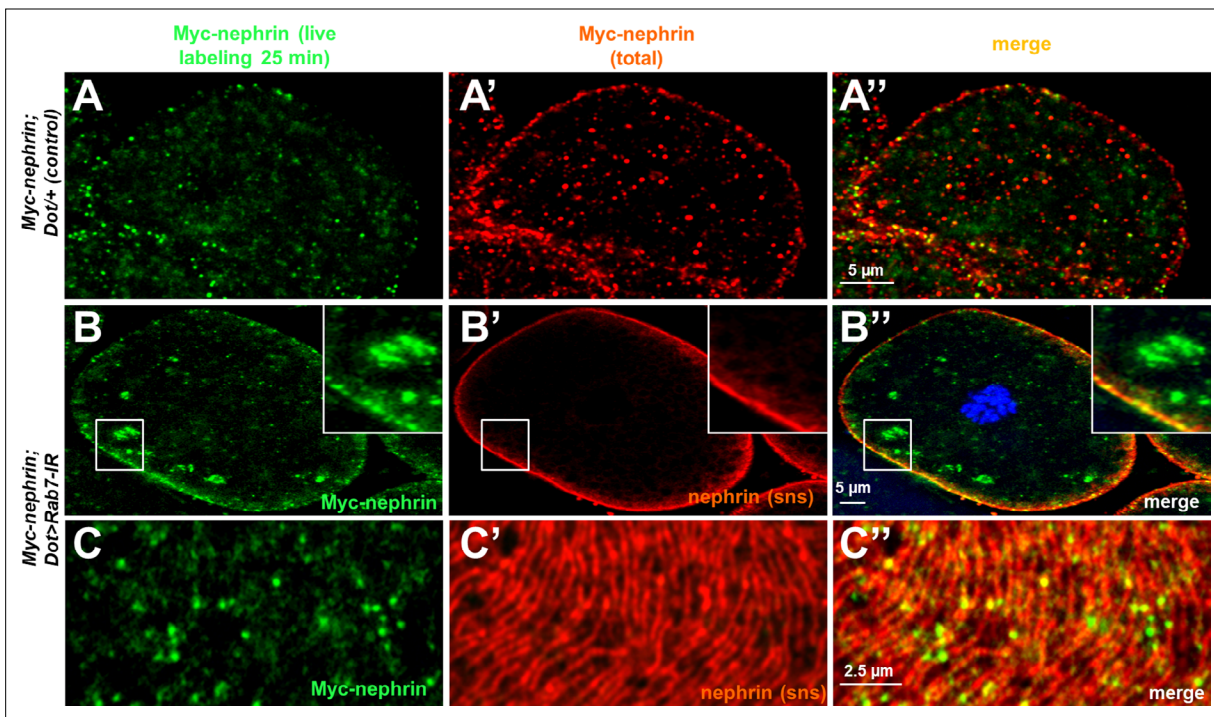


Figure 5—figure supplement 2. Additional images for live antibody. (A–A'') Confocal images of control nephrocytes that express Myc-nephrin heterozygously show complete turnover, not distinguishable from cells that carry the genom-edited locus homozygously (compare to **Figure 2**). (B–C'') Confocal images of nephrocyte expressing *Rab7*-RNAi after live antibody labeling show subcortical vesicles that exclusively stain for the live labeled antibody (green) but not for nephrin staining, suggesting they contain antibody that is no longer coupled to nephrin (B–B''). Tangential sections from the same cell confirm undisturbed nephrin turnover as the live labeled antibody is removed from the surface (C–C''). Nuclei are marked by Hoechst 33342 in blue here and throughout the figure.

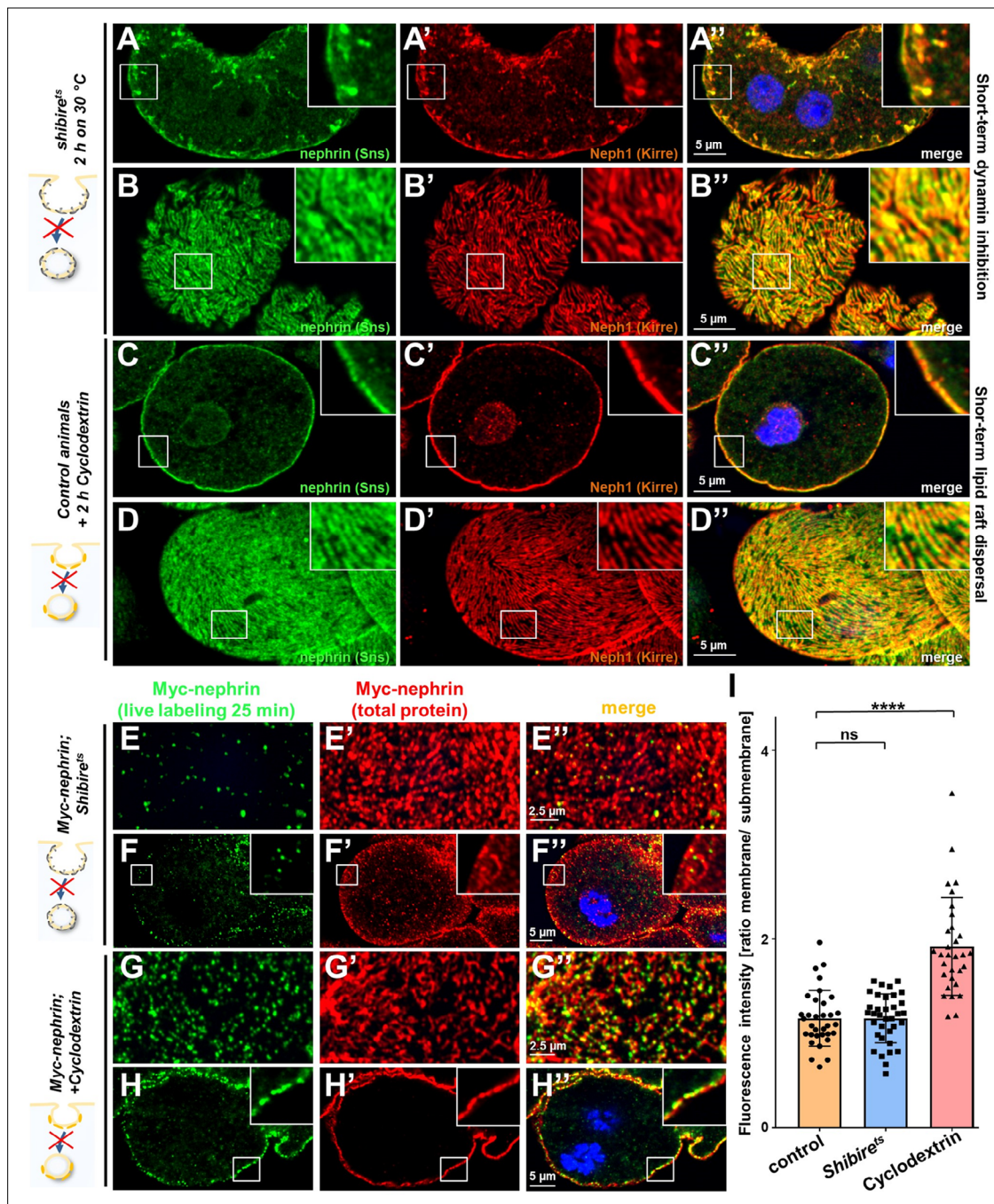


Figure 6. Differential transport through dynamin-mediated or raft-mediated endocytosis is required for slit diaphragm maintenance in nephrocytes. (A–B”) Confocal images of nephrocytes stained for slit diaphragm proteins carrying a temperature-sensitive variant (*G141S*) of *shibire*, the *Drosophila* dynamin, homozygously. The mutant protein is functional at lower temperatures but lacks function at 30°C and the animals were exposed to 30°C for 2 hr before staining. Cross sections show accumulation of subcortical slit diaphragm protein in clusters and short lines protruding from the surface (A–A”). Tangential sections indicate a mild confluence and few brighter clusters of slit diaphragm proteins (B–B”). (C–D”) Confocal images of control nephrocytes treated with cyclodextrin for 2 hr ex vivo to inhibit raft-mediated endocytosis show a regular staining pattern of slit diaphragm proteins in cross-sectional (C–C”) and tangential planes (D–D”). (E–H”) Confocal microscopy images showing tangential sections (panels E and G) and cross sections (panels F and H) of nephrocytes carrying one copy of the genomic Myc-nephrin after live antibody labeling with 2 hr of chase period are for the indicated genotypes or interventions. *Shibire^{ts}* animals show intense nephrocyte turnover in the live labeling assay despite exposure to a temperature of 31°C for 2 hr which inhibits function of the fly dynamin during that period (E–F”). In contrast, blocking raft-mediated endocytosis for 2 hr by cyclodextrin in control nephrocytes strongly diminishes nephrin turnover and a large amount of the live labeled antibody is retained (G–H”). This suggests that nephrin turnover depends on raft-mediated endocytosis that occurs independent from dynamin function. The diffuse intracellular signal

Figure 6 continued on next page

Figure 6 continued

from live labeling was similar to control (**Figure 5—figure supplement 2A**). (I) Quantitation of results from (**E–H**) expressed as ratio of the fluorescence intensity between surface and subcortical region for individual cells (mean \pm standard deviation, $n=11–12$ animals per genotype, $p>0.05$ for *shibire^{ts}*, and $p<0.0001$ for cyclodextrin treatment).

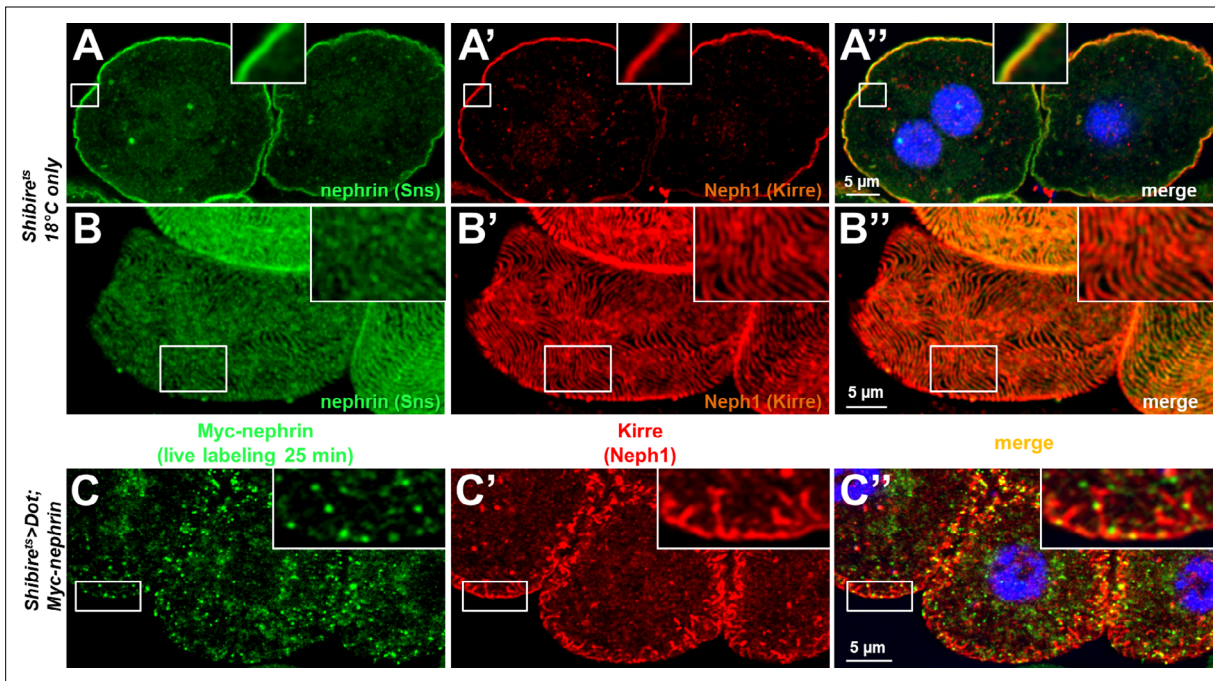


Figure 6—figure supplement 1. Validation and controls for *Shibire^{ts}*. (A–B'') Nephrocytes carrying the temperature-sensitive allele of *shibire* show a regular staining pattern at a lower temperature at which the protein remains functional in cross sections (A–A'') and tangential sections (B–B''). (C–C'') A chase time of 120 min after live antibody labeling is shown for the temperature-sensitive allele of *shibire* with Kirre co-staining. Most of the live labeled nephrin is removed from the cell surface while Kirre indicates a severe mislocalization.

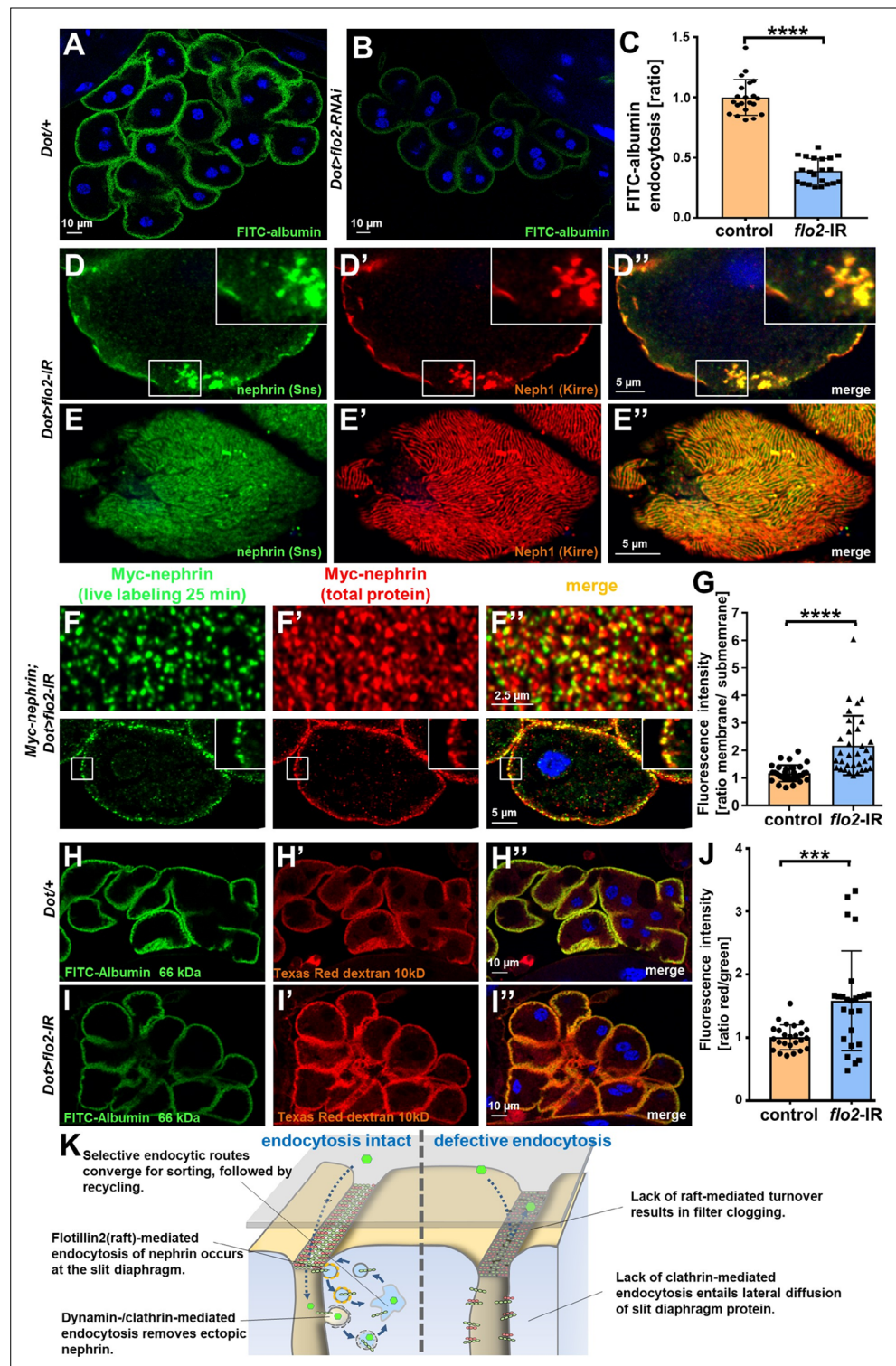


Figure 7. Flotillin2-mediated endocytosis is required for nephrin turnover in *Drosophila* nephrocytes. (A–B) Confocal microscopy images of nephrocytes after uptake of FITC-albumin as read-out of nephrocyte function are shown. Control nephrocytes exhibit stronger uptake (A) than nephrocytes expressing *flo2*-RNAi (B). (C) Quantitation of results analogous to (A–B) in ratio to a control experiment performed in parallel (mean ± standard deviation, n=7 animals per genotype, p<0.0001 for *flo2*-RNAi). (D–E’’) Confocal images of nephrocytes expressing *flo2*-RNAi show localized breakdown of slit diaphragms in cross-sectional (D–D’’) and tangential planes (E–E’’) (F–F’’) Confocal microscopy images in tangential sections (upper row) and cross sections (lower row) of nephrocytes

Figure 7 continued on next page

Figure 7 continued

are shown after live antibody labeling with 2 hr of chasing. Animals express *flo2*-RNAi under control of *Dorothy-GAL4*. Nephrin turnover is strongly reduced compared to control (**Figure 5—figure supplement 2A**). The diffuse intracellular signal from live labeling was similar to control (**Figure 5—figure supplement 2A**). (**G**) Quantitation of results from (**F**) compared to control experiments. Results are expressed as ratio of the fluorescence intensity between surface and subcortical regions for individual cells (mean \pm standard deviation, $n=11$ animals per genotype, $p<0.0001$ for *flo2*-RNAi). (**H–I'**) Confocal microscopy images of nephrocytes after simultaneous uptake of FITC-albumin (66 kDa, green) and Texas-Red-Dextran (10 kDa) are shown. Control nephrocytes show significant uptake of both tracers (**H–H'**). Silencing of *flo2* causes a stronger decrease in the uptake of the larger tracer FITC-albumin compared to smaller Texas-Red-Dextran (**I–I'**). (**J**) Quantitation of fluorescence intensity expressed as a ratio of Texas-Red-Dextran/FITC-albumin (small/large tracer) confirms a disproportionate reduction for *flo2*-RNAi (mean \pm standard deviation, $n=9$ animals per genotype, $p<0.001$ for *flo2*-RNAi). (**K**) Schematic illustrating the proposed mechanistic role of endocytosis for maintenance of the filtration barrier. Left: Ectopic fly nephrin within the channels is removed by clathrin-dependent endocytosis that returns most of the protein to the surface through recycling pathways. The nephrin that is bound within the slit diaphragm complex is subject to turnover in a shorter circuit that is raft-mediated and feeds into recycling as well. Right: Upon disruption of endocytosis filtration is impaired by clogging of the filter due to lack of cleansing and the architecture of the slit diaphragms is disturbed by unhindered lateral diffusion of slit diaphragm protein.

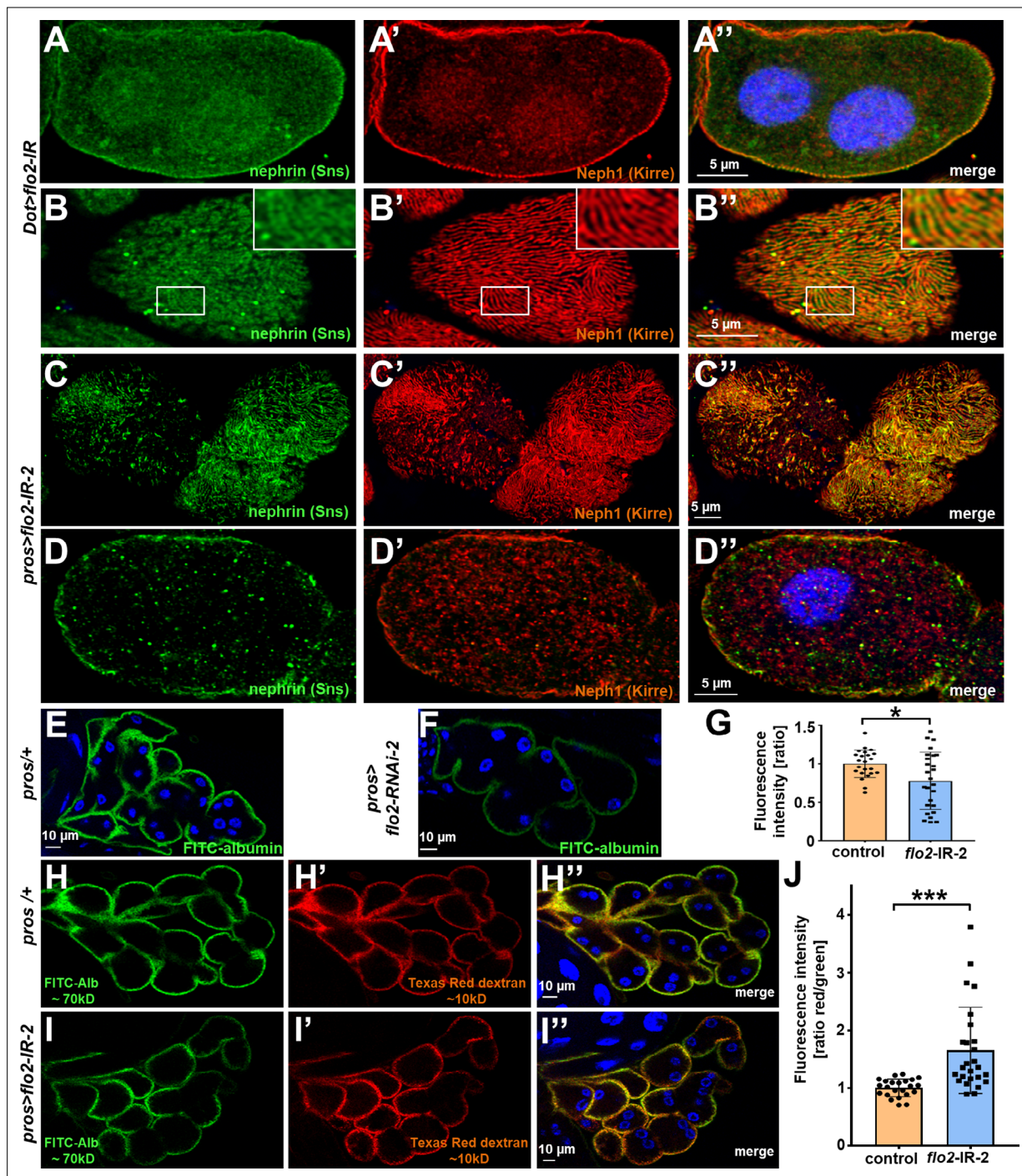


Figure 7—figure supplement 1. Silencing flotillin2 using a second RNAi line confirms reduced FITC-albumin uptake and altered permeability of the filtration barrier. (A–D) Silencing of *flo2* may result in regular nephrin/Neph1 staining (A–B, using *flo2*-RNAi 1) or localized breakdown of slit diaphragm (C–D, using *flo2*-RNAi 2). Nuclei are marked by Hoechst 33342 in blue here and throughout the figure. (E–F) Confocal microscopy image of nephrocytes after uptake of FITC-albumin shows impaired uptake of nephrocytes expressing *flo2*-RNAi-2 (F) compared to control cells (E). (G) Quantitation of results from (E–F) in ratio to a control experiment performed in parallel (mean \pm standard deviation n=8–9 animals per genotype, $p < 0.05$ for *flo2*-RNAi-2). (H–I'') Confocal microscopy image of nephrocytes after simultaneous uptake of FITC-albumin (66 kDa, green) and the smaller endocytic tracer Texas-Red-Dextran (10 kDa) are shown. Silencing of *flo2* causes a relatively stronger decrease in the uptake of the larger tracer FITC-albumin compared to smaller Texas-Red-Dextran. (J) Quantitation of fluorescence intensity expressed as a ratio of Texas-Red-Dextran/FITC-albumin (small/large tracer) confirms a disproportionate reduction for *flo2*-RNAi-2 (mean \pm standard deviation, n=8–9 animals per genotype, $p < 0.001$ for *flo2*-RNAi-2).